FLUORESCENCE MICROSCOPY IMAGING DENOISING WITH LOG-EUCLIDEAN PRIORS AND PHOTOBLEACHING COMPENSATION

[1,2]*Isabel Rodrigues and* [2,3]*João Sanches*

Instituto Superior de Engenharia de Lisboa, Lisbon[1]
Instituto de Sistemas e Robótica, Lisbon[2]
Instituto Superior Técnico, Lisbon[3]

ABSTRACT

Fluorescent protein microscopy imaging is nowadays one of the most important tools in biomedical research. However, the resulting images present a low *signal to noise ratio* and a time intensity decay due to the *photobleaching* effect. This phenomenon is a consequence of the decreasing on the radiation emission efficiency of the tagging protein. This occurs because the fluorophore permanently loses its ability to fluoresce, due to photochemical reactions induced by the incident light. The Poisson multiplicative noise that corrupts these images, in addition with its quality degradation due to *photobleaching*, make long time biological observation processes very difficult.

In this paper a denoising algorithm for Poisson data, where the *photobleaching* effect is explicitly taken into account, is described. The algorithm is designed in a Bayesian framework where the data fidelity term models the Poisson noise generation process as well as the exponential intensity decay caused by the *photobleaching*. The prior term is conceived with Gibbs priors and *log-Euclidean* potential functions, suitable to cope with the positivity constrained nature of the parameters to be estimated.

Monte Carlo tests with synthetic data are presented to characterize the performance of the algorithm. One example with real data is included to illustrate its application.

Index Terms— Photobleaching, Poisson Denoising, Bayesian, Total Variation, Log-Euclidean Potentials.

1. INTRODUCTION

Fluorescence microscopy imaging became a fundamental tool in biological, medical, pharmaceutical and chemical research since it allows the study of the dynamics of living cells in an almost non-invasive manner.

The phenomenon of fluorescence in certain specific substances consists on the emission of radiation with a longer wavelength than the one of the incident radiation, by excited molecules within nanoseconds after the absorption of photons. The fluorophore is the component of the molecule responsible for its capability to fluoresce and it is able to maintain for a long time triplet excited states that favour the occurrence of photochemical reactions that irreversibly destroy its fluorescence and/or cause phototoxicity [1]. This phenomenon is called the *photobleaching* effect. Upon extended excitation all the fluorophores will eventually photobleach. Since illumination is needed to excite and observe the tagging fluorescent proteins in the specimen, the acquisition of this type of images becomes a hard task for long exposures. One way to obviate this effect is to reduce the intensity of the incident radiation. However, this strategy leads to a decreasing in the *signal to noise ratio* of the acquired images. This is not the only difficulty one has to deal with. The fluorescence microscopy images may be considered of photon-limited type due to the small amount of detected radiation and to the huge optical and electronic amplification they are put through. Thus they are usually corrupted by a severe type of multiplicative noise described by a Poisson distribution.

In this paper a denoising algorithm for Poisson data that explicitly takes into account the global *photobleaching* effect is presented. The goal is to estimate the basic morphology and the rate of intensity decay due to *photobleaching* of fluorescence microscopy images of human cells.

Different types of photobleaching curves are considered in the literature [2], [3] and among them the most commonly used are the ones presenting an exponential decaying behaviour (mono- or multi-negative exponentials). Here the intensity decrease along the time is modeled using a mono-exponential decaying approach with a constant rate which corresponds to the assumption of a homogeneous fluorophore population. It is also assumed that the morphology of the cell nucleus under observation is allowed to vary in space following a pattern that consists of sets of homogeneous regions separated by well defined boundaries, but not in time, so the overall intensity decay in the set of images could be revealed through the exponential term.

The algorithm is formulated in a Bayesian framework as an optimization task where a convex energy function is minimized. *Maximum a posteriori* (MAP) estimation is employed since it has been successfully used and is well-suited to image restoration. Nevertheless the denoising of fluorescence microscopy images is in general an ill-posed and an ill-conditioned problem [4] requiring some sort of regularization that in the Bayesian framework is expressed in the form of *a prior* distribution functions. Given the characteristics of these images, the local Markovianity of the nucleus morphology seams to be a reasonable assumption thus, according to the Hammersley-Clifford theorem [5], a Gibbs distribution with appropriate potentials can be considered as *a prior* for the base morphology. Several potentials have been proposed in the literature [6, 7]. One of the most popular of these functions is the quadratic, mainly for the sake of mathematic simplicity. However this function oversmooths the solution. An alternative is the use of *edge preserving priors* such as *total variation* (TV) based Gibbs energy ones that have been successfully used in several problems [7, 8, 9]. Very recently a new type of potential functions was proposed in [10]. This approach is based on log-Euclidean norms and instead of using differences between neighbors, uses logarithms of their ratios which means differences of logarithms, allowing the interpretation of differences between neighbors in terms of the order of magnitude. This new approach is suitable to be used here due to the positiveness of the unknowns to be estimated.

Correspondent author: Isabel Rodrigues (irodrigues@isr.ist.utl.pt). This work was supported by Fundação para a Ciência e a Tecnologia (ISR/IST plurianual funding) through the POS Conhecimento Program which includes FEDER funds.

Synthetic data were generated with a low level of *signal to noise ratio* and a Monte Carlo experiment was carried on with these data in order to evaluate the performance of the algorithm.

Real data of a HeLa immortal cell [11] nucleus, acquired by a laser scanning fluorescence confocal microscope (LSFCM), are used to illustrate the application of the algorithm.

2. PROBLEM FORMULATION

Each sequence of fluorescence microscopy $N \times M$ images under analysis , $\mathbf{Y}$, corresponds to L observations of a cell nucleus acquired along the time. Data can be represented by a 3D tensor, $\mathbf{Y} = \{y_{i,j,t}\}$, with $0 \leq i,j,t \leq N-1, M-1, L-1$. Each data point, $y_{i,j,t}$, is corrupted by Poisson noise and the time intensity decrease due to the *photobleaching* effect is modeled by a decaying exponential whose rate, denoted by λ, is supposed to be constant along the time t and in space (i,j). The constancy of this rate in space is a reasonable assumption in situations when the background and the nucleus are identified, for instance through a segmentation procedure using graph-cuts, and the population inside the nucleus is considered as homogeneous. Each point of the noiseless cell nucleus images, $\mathbf{X}$, can then be written as

$$x_{i,j,t} = f_{i,j} e^{-\lambda t} \tag{1}$$

where $\mathbf{F} = \{f_{i,j}\}$, with $0 \leq i,j \leq N-1, M-1$ stands for the underlying morphology of the cell nucleus. This morphology is assumed to be a sole function of the position in the image, since the purpose of this approach is that all the time variability in the intensity of the images could be caught by the exponential term.

The ultimate goal of the proposed algorithms is to estimate the cell nucleus underlying morphology, $\mathbf{F}$, and the rate of decay, λ, from these noisy data, $\mathbf{Y}$, exhibiting a very low *signal to noise ratio* (SNR). A Bayesian approach using the *maximum a posteriori* (MAP) criterion is adopted to estimate $\mathbf{F}$ and λ. This problem may be formulated as the following energy optimization task

$$(\hat{\mathbf{F}}, \hat{\lambda}) = \arg\min_{\mathbf{F},\lambda} E(\mathbf{F}, \lambda, \mathbf{Y}) \tag{2}$$

where the energy function $E(\mathbf{F}, \lambda, \mathbf{Y}) = E_Y(\mathbf{F}, \lambda, \mathbf{Y}) + E_F(\mathbf{F})$ is a sum of two terms, $E_Y(\mathbf{F}, \lambda, \mathbf{Y})$ called the *data fidelity term* and $E_F(\mathbf{F})$ called the energy associated to the *a prior* distribution for $\mathbf{F}$. The *a prior* information for λ is merely its overall constancy. The first term pushes the solution towards the observations according to the type of noise corrupting the images and the *a prior* energy term penalizes the solution in agreement with some previous knowledge about $\mathbf{F}$, in this case a stepwise function [12].

Assuming the independence of the observations, the *data fidelity term*, which is the negative of the log-likelihood function, is defined as

$$E_Y(\mathbf{F}, \lambda, \mathbf{Y}) = -\log\left[\prod_{i,j,t=0}^{N-1,M-1,L-1} p(y_{i,j,t}|f_{i,j}, \lambda)\right], \tag{3}$$

where $p(y|f,\lambda) = \frac{(f_{i,j}\exp(-\lambda t))^y}{y!} e^{-(f_{i,j}\exp(-\lambda t))}$ is the Poisson distribution, yielding

$$E_Y(\mathbf{F}, \lambda, \mathbf{Y}) = \sum_{i,j,t=0} \left[f_{i,j}e^{-\lambda t} - y_{i,j,t}\log\left(f_{i,j}e^{-\lambda t}\right)\right] + C \tag{4}$$

and C is a constant term.

The prior term regularizes the solution and helps to remove the noise. By assuming $\mathbf{F}$ as *Markov Random Field* (MRF), $p(\mathbf{F})$ can be written as a Gibbs distribution, $p(\mathbf{f}) = \frac{1}{Z}\exp[-\sum_{c\in C} V_c(\mathbf{f})]$,

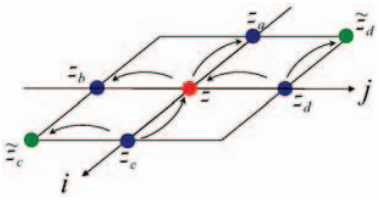

Fig. 1. Neighboring system.

where Z is the normalizing constant and $V_c(.)$ are the *clique potentials* [13]. The negative of the argument of the exponential function is called *energy* and will be denoted by $E_F(\mathbf{F})$. The choice of the potential functions to be used in each problem is a very important step because they act upon the solution. In this paper *log*-Euclidean [10] based potential functions are used. These functions, that can be interpreted as *log-total variation* potentials, produce edge-preserving priors which are the most convenient to preserve the edges of the cell nucleus morphology. The energy function related to the *a priori* distribution is given by:

$$E_F(F) = \alpha \sum_{i,j,t} \sqrt{\log^2\left(\frac{f_{i,j}}{f_{i-1,j}}\right) + \log^2\left(\frac{f_{i,j}}{f_{i,j-1}}\right)} \tag{5}$$

Therefore the overall problem consists on the minimization of the following function

$$\begin{aligned} E(\mathbf{F}, \lambda, \mathbf{Y}) &= \sum_{i,j,t}\left[f_{i,j}e^{-\lambda t} - y_{i,j,t}(\log(f_{i,j}) - \lambda t)\right] \\ &+ \alpha L \sum_{i,j} \sqrt{\log^2\left(\frac{f_{i,j}}{f_{i-1,j}}\right) + \log^2\left(\frac{f_{i,j}}{f_{i,j-1}}\right)} \end{aligned} \tag{6}$$

This optimization task leads to a non-convex problem [14] since it involves sums of convex functions with concave ones *e.g.* $\sqrt{\log^2(x)}$, rendering the use of *gradient descendant* or Newton-Raphson based methods difficult. However, performing an appropriate change of variable, $z = g(f) = log(f)$, it is possible to turn it into convex. The minimizers of $E(\mathbf{F}, \lambda, \mathbf{Y})$ in $\mathbf{F}$ and of $E(\mathbf{Z}, \lambda, \mathbf{Y})$ in $\mathbf{Z}$ are related by $\mathbf{Z}^* = \log(\mathbf{F}^*)$ due to the monotonicity of function $g(f)$. The new objective function for this model is

$$\begin{aligned} E(\mathbf{Z}, \lambda, \mathbf{Y}) &= \sum_{i,j,t}\left[e^{z_{i,j}-\lambda t} - y_{i,j,t}(-z_{i,j} + \lambda t)\right] \\ &+ \alpha L \sum_{i,j} \sqrt{(z_{i,j} - z_{i-1,j})^2 + (z_{i,j} - z_{i,j-1})^2} \end{aligned} \tag{7}$$

The minimization of (7) is accomplished by finding its stationary points, performing iteratively its optimization in Z with respect to each component $z_{i,j}$ one at a time, considering all other components as constants in each iteration. Let us now consider only the terms involving a given node $z = z_{i,j}$ in the energy function (7),

$$\begin{aligned} E(z, \lambda, y) = \sum_t (e^{z-\lambda t} - yz) + \alpha L[&\sqrt{(z - z_a)^2 + (z - z_b)^2} \\ &+ \sqrt{(z_c - z)^2 + (z_c - \tilde{z}_c)^2} + \sqrt{(z_d - \tilde{z}_d)^2 + (z_d - z)^2}] + C \end{aligned} \tag{8}$$

where z_a, z_b, z_c, z_d are the neighbors of z and $\tilde{z}_c$ and $\tilde{z}_d$ are neighbors of z_c and z_d respectively as shown in Fig.1; C is a term that does not depend on z. The *reweighted least squares* (RWLS) method [12, 15] is used to obviate the numerical difficulties introduced by the

non-quadratic TV terms. The minimizer of the convex energy function (8), z^*, is also the minimizer of the following energy function with quadratic terms associated with the spatial interaction

$$\tilde{E}(z,\lambda,y,z^*) = e^{z-\lambda t} - yz + \alpha L[w(z^*)((z-z_a)^2+(z-z_b)^2) + w_c(z^*)((z_c-z)^2+(z_c-\tilde{z}_c)^2) + w_d(z^*)((z_d-\tilde{z}_d)^2+(z_d-z)^2)] \quad (9)$$

where $w(z) = \frac{1}{\sqrt{(z-z_a)^2+(z-z_b)^2}}$, $w_c(z) = \frac{1}{\sqrt{(z_c-z)^2+(z_c-\tilde{z}_c)^2}}$ and $w_d(z) = \frac{1}{\sqrt{(z_d-\tilde{z}_d)^2+(z_d-z)^2}}$.

Since the weights $w(z^*)$, $w_c(z^*)$ and $w_d(z^*)$ depend on z^*, which is not known, an iterative procedure is used where in each k^{th} iteration the previous estimation of z^*, z^{k-1}, is used to compute them. Let us denote $w(z^{k-1})$, $w_c(z^{k-1})$ and $w_d(z^{k-1})$, calculated at node (i,j), simply by w, w_c and w_d. The minimization of the resulting energy function with respect to $z_{i,j}$ is accomplished by finding its stationary point, which is equivalent to solve the equation

$$\sum_t (e^{z_{i,j}-\lambda t} - y) + h_{i,j} = 0 \quad (10)$$

where $h_{i,j} = 2\alpha L[(2w + w_c + w_d)z_{i,j} - w\,(z_{i-1,j} + z_{i,j-1}) - w_c z_{i+1,j} - w_d z_{i,j+1}]$. The minimization of the energy function with respect to λ (the rate of decay due to the *photobleaching* effect) is performed by computing the zero of

$$\sum_t (-te^{z_{i,j}-\lambda t} - y_{i,j,t}t) = 0 \quad (11)$$

Using the Newton-Raphson method the solution of (10) and (11) is obtained in each iteration by

$$z_{i,j}^{(k+1)} = z_{i,j}^{(k)} - \frac{\sum_t (e^{z_{i,j}-\lambda t} - y_{i,j,t}) + h_{i,j}}{\sum_t (e^{z_{i,j}-\lambda t}) + 2\alpha L(2w + w_c + w_d)} \quad (12)$$

and

$$\lambda^{(k+1)} = \lambda^{(k)} - \frac{\sum_{i,j,t}(-te^{z_{i,j}-\lambda t} + y_{i,j,t}t)}{\sum_{i,j,t}(t^2 e^{z_{i,j}-\lambda t})}. \quad (13)$$

Reversing the change of the variable $\mathbf{Z}$, the final solution for the underlying morphology is

$$\hat{\mathbf{F}} = e^{\hat{\mathbf{Z}}}. \quad (14)$$

3. EXPERIMENTAL RESULTS

In this section, results using synthetic and real data are presented. The synthetic data is used to characterize the performance of the denoising algorithm. A real images sequence is employed to illustrate the application of the algorithm to estimate the underlying morphology of a HeLa cell nucleus.

3.1. Synthetic Data

Results of a Monte Carlo experiment are presented in order to access the performance of the proposed algorithm. A 64×64 pixels synthetic underlying morphology image was generated and an exponential decay along the time, $t = (0, ..., 63)$, with rate $\lambda = 0.01$, was applied upon it to simulate the global *photobleaching*. The Monte Carlo experiment was then carried out in 500 runs with 500 iterations each, which took a time of 18s *per* run in a Centrino Duo 2.00GHz, 1.99 GB RAM processor. In each run the sequence was corrupted with Poisson noise. Since this type of noise is multiplicative, the underlying morphology intensities were previously chosen in order to achieve initial *signal to noise ratio* values in the range $[-1, 2]$ dB along the sequence. The derived synthetic data were then processed using the algorithm described in the paper with regularization parameter $\alpha = 1$. The reconstruction *mean square error* ($MSE_{\hat{\mathbf{X}}}$) and the *Signal to noise ratio* (SNR) were computed for each image and run. The Csiszár's I-divergence [16], used here to measure the discrepancy of image $\mathbf{U}(t)$ with respect to $\mathbf{X}(t)$, is defined as follows

$$\text{I-div}(\mathbf{X}(t), \mathbf{U}(t)) = \sum_{i,j} \left[x_{i,j,t} \log\left(\frac{x_{i,j,t}}{u_{i,j,t}}\right) - x_{i,j,t} + u_{i,j,t} \right] \quad (15)$$

where $\mathbf{U}(t)$ is the the noisy sequence $\mathbf{Y}(t)$ and the estimated denoised one $\hat{\mathbf{X}}(t)$, to measure the improvement. The MSE for the underlying morphology, $MSE_{\mathbf{F}}$, and for the rate of decay, MSE_λ, were also computed in each run. The mean values and the standard deviations of each *figure of merit* are computed from the 500 results of the Monte Carlo test and displayed. Plots of the initial and final SNR and of the *I-divergence* together with the curve of the $MSE_{\hat{\mathbf{X}}}$ as a function of time (image) are represented in Fig. 2. The thinner lines above and below each curve of the computed means of the *figures of merit* stand for error bounds obtained by addition and subtraction of the respective values of the standard deviations. As shown in the plots, the SNR improvement attains values of almost $30dB$ which is in perfect agreement with the decrease in the I-div. The $MSE_{\hat{\mathbf{X}}}$ exhibits low values, the same occurring for $MSE_{\mathbf{F}} = 0.0395$ and $MSE_\lambda = 1.17 \times 10^{-5}$. These results suggest that the obtained estimates are very close to the originals. Fig. 3 shows the original (a),(d), the noisy (b),(e) and the reconstruction (c),(f) versions of the first image of the synthetic sequence. In the same Fig. are plotted the respective profiles of intensity (g). Fig. 3 corresponds in fact to the underlying morphology since for $t = 0$ (first image of the sequence) the exponential term is 1. The edge preserving capabilities of the algorithm are noticeable in the mesh representations and even better in the profile plots.

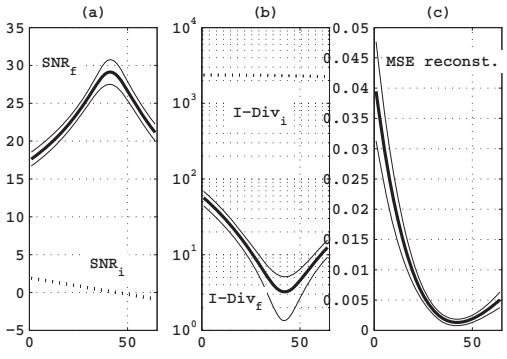

Fig. 2. Result of the Monte Carlo experiment: (a) SNR curves before (initial) and after (final) applying the algorithm and respective error bounds. (b) Csiszár's I-divergence curves before (initial) and after (final) applying the algorithm and respective error bounds.(c) Mean Square Error of the reconstruction and respective error bounds.

3.2. Real Data

The sequence used to show the application of the algorithm described in the paper to real data is the result of the acquisition of 100 images of the HeLa cell nucleus in a laser scanning fluorescence confocal microscope through the green channel. This sequence is represented by a 3-D tensor $\mathbf{Y}$, as described in Section 2. On these images a simple alignment procedure was performed to correct for

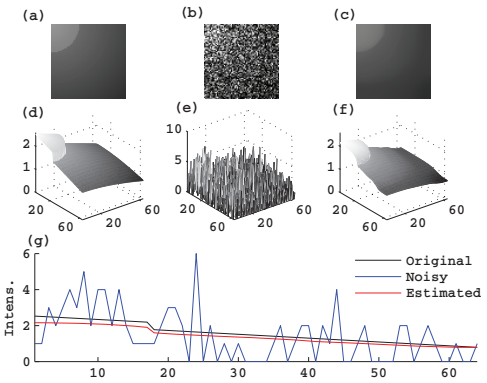

Fig. 3. Image 1 of the sequence of synthetic data (underlying morphology): (a),(d) Original. (b),(e) Noisy. (c),(f) Estimated. (g) Intensity profiles.

cell nucleus displacement during the acquisition process. The alignment consists in a set of rigid body transformations driven by the maximization of the correlation between images, using a wavelet based strategy. The results of the use of the presented denoising procedure are shown in Fig. 4 where (a), (c) stand for raw data image 50 (from a sequence of 100 images) and its mesh and (b), (d) show the estimated underlying morphology and the respective mesh representation. Image 50 is shown just to give the reader some insight on the difficulty of using such a low quality image in a biological research. Notice that with this method it is possible to recover with a high quality an image of the underlying anatomy without using to much radiation that could cause injuries or even death to the cell due to the *phototoxicity*.

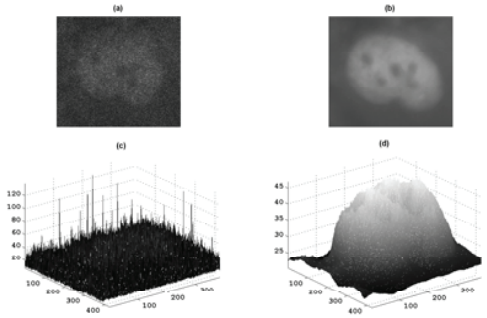

Fig. 4. Real data:(a),(c) Noisy image 50. (b),(d) Estimated underlying morphology ($\hat{\lambda} = 0.0077$). Data provided by the Molecular Medicine Institute of Lisbon, Portugal.

4. CONCLUDING REMARKS

In this paper a new denoising algorithm for Poisson data resulting from fluorescence microscopy (FM) imaging is proposed. The sequences of images taken along the time, in this microscopy image modality, are corrupted by a type of multiplicative noise described by a Poisson distribution. Furthermore, the global intensity of the images decreases along the time due to permanent fluorophore loss of its ability to fluoresce, caused by photochemical reactions induced by the incident light (*photobleaching* effect). The decreasing on the image intensity leads to a decreasing on the *signal to noise ratio* of the images, making the biological information recovery a difficult task. In the proposed algorithm this effect is explicitly taken into account.

This approach is conceived as an optimization task with the *maximum a posteriori* (MAP) criterion. The energy functions are designed to be convex and their minimizers are computed by using the Newtons's algorithm to estimate the rate of decay, assuming a negative mono-exponential to model the *photobleaching* and the Newton's algorithm and a reweighted least squares based method in the estimation procedure of the morphology of the cell nucleus, which allows continuous convergence toward the global minimum, in a small number of iterations.

Monte Carlo tests with synthetic data were used to assess the performance of the algorithm. These tests have shown the ability of the algorithm to strongly reduce the Poisson multiplicative noise and to estimate the underlying morphology. The main characteristic of the algorithm is its ability to used all the information, even the last images of the sequence with a very low SNR, to recover the cell morphology.

Tests with real data from *fluorescence confocal microscopy* were also performed where it is shown the effectiveness of the algorithm to cope with this type of noise and low SNR. Its performance is related to the use of edge preserving *a prior* to model the prior knowledge about the cell morphology that is assumed to be stepwise constant.

5. REFERENCES

[1] J. W. Lichtman and J. A. Conchello, "Fluorescence microscopy," *Nature Methods*, vol. 2, pp. 910 – 919, 2005.

[2] N. B. Vicente, J. E. D. Zamboni, J. F. Adur, E. V. Paravani, and V. H. Casco, "Photobleaching correction in fluorescence microscopy images," *Journal of Physics: Conference Series*, vol. 90, no. 012068, pp. 1 – 8, 2007.

[3] R. Zondervan, F. Kulzer, M. A. Kol'chenco, and M. Orrit, "Photobleaching of rhodamine 6g in poly(vinyl alcohol) at the ensemble and single-molecule levels," *J. Phys. Chem. A*, vol. 108, pp. 1657 – 1665, 2004.

[4] C. Vogel and M. Oman, "Fast, robust total variation-based reconstruction of noisy, blurred images," *IEEE Transactions on Image Processing*, vol. 7, no. 7, pp. 813–824, 1998.

[5] J. Besag, "On the statistical analysis of dirty pictures," *J. R. Statist. Soc. B*, vol. 48, no. 3, pp. 259–302, 1986.

[6] T. Hebert and R. Leahy, "A generalized EM algorithm for 3-d bayesian reconstruction from Poisson data using Gibbs priors," *IEEE Transactions on Medical Imaging*, vol. 8, no. 12, pp. 194 – 202, 1989.

[7] S.Osher L.Rudin and E. Fatemi, "Nonlinear total variation based noise removal algorithms," *Physica D*, vol. 60, pp. 259–268, 1992.

[8] J.Bardsley and A.Luttman, "Total variation-penalized Poisson likelihood estimation for ill-posed problems," Tech. Rep. 8, Depart. Math Sci., Univ. Montana Missoula, 2006.

[9] N. Dey, L. Blanc-Feraud, C. Zimmer, Z. Kam, J.-C. Olivo-Marin, and J. Zerubia, "A deconvolution method for confocal microscopy with total variation regularization," *IEEE International Symposium on Biomedical Imaging: Nano to Macro, 2004*, vol. 2, pp. 1223–1226, April 2004.

[10] V. Arsigny, P. Fillard, X. Pennec, and N. Ayache, "Log-Euclidean metrics for fast and simple calculus on diffusion tensors," *Magnetic Resonance in Medicine*, vol. 56, no. 2, pp. 411–421, August 2006.

[11] D. Jackson, F. Iborra, E. Manders, and P. Cook., "Numbers and organization of rna polymerases, nascent transcripts, and transcription units in hela nuclei.," *Mol Biol Cell*, vol. 9, pp. 1523–1536, 1998.

[12] T.Moon and W. Stirling, *Mathematical methods and algorithms for signal processing*, Prentice-Hall, 2000.

[13] S. Geman and D. Geman, "Stochastic relaxation, Gibbs distributions, and the bayesian restoration of images," *IEEE Transactions on Pattern Analysis and Machine Intelligence*, vol. PAMI, no. 6, pp. 721–741, Nov. 1984.

[14] L. Boyd, S.and Vandenberghe, *Convex Optimization*, Cambridge University Press, March 2004.

[15] Brendt Wohlberg and Paul Rodríguez, "An iteratively reweighted norm algorithm for minimization of total variation functionals," *IEEE Signal Processing Letters*, vol. 14, no. 12, pp. 948 – 951, 2007.

[16] I. Csiszar, "Why least squares and maximum entropy? An axiomatic approach to inference for linear inverse problems," *The Annals of Statistics*, vol. 19, no. 4, pp. 2032–2066, 1991.